

# Development of a Molecular Model for Understanding the Polymer-metal Interface in Solid State Pumps

Jaime D. Guevara

Micron School of Materials Science and Engineering  
Boise State University  
Boise, ID  
jaimeguevara@u.boisestate.edu

Peter Müllner

Micron School of Materials Science and Engineering  
Boise State University  
Boise, ID  
petermullner@boisestate.edu

Matthew L. Jones

Micron School of Materials Science and Engineering  
Boise State University  
Boise, ID  
MattyJones@boisestate.edu

Eric Jankowski\*

Micron School of Materials Science and Engineering  
Boise State University  
Boise, ID  
ericjankowski@boisestate.edu

## ABSTRACT

Medical micropumps that utilize Magnetic Shape Memory (MSM) alloys are small, powerful alternatives to conventional pumps because of their unique pumping mechanism. This mechanism—the transfer of fluid through the emulation of peristaltic contractions—is enabled by the magneto-mechanical properties of a shape memory alloy and a sealant material. Because the adhesion between the sealant and the alloy determines the performance of the pump and because the nature of this interface is not well characterized, an understanding of sealant-alloy interactions represents a fundamental component of engineering better solid state micropumps in particular, and metal-polymer interfaces in general. In this work we develop computational modeling techniques for investigating how the properties of sealant materials determine their adhesive properties with alloys. Specifically, we develop a molecular model of the sealant material polydimethylsiloxane (PDMS) and characterize its behavior with a model Ni-Mn-Ga surface. We perform equilibrium molecular dynamics simulations of the PDMS/Ni-Mn-Ga interface to iteratively improve the reliability, numerical stability, and accuracy of our models and the associated data workflow. To this end, we develop the first model for simulating PDMS/Ni-Mn-Ga interfaces by combining the Optimized Potentials for Liquid Simulations (OPLS) [21] force field with the Universal Force Field [5], and show promise for informing the design of more reliable MSM micropumps. We also reflect on the experiences of Blue Waters Supercomputing intern Guevara (the first author) to identify key learning moments during the one-year internship that can help guide future molecular simulation training efforts.

\*Corresponding author

Permission to make digital or hard copies of all or part of this work for personal or classroom use is granted without fee provided that copies are not made or distributed for profit or commercial advantage and that copies bear this notice and the full citation on the first page. To copy otherwise, or republish, to post on servers or to redistribute to lists, requires prior specific permission and/or a fee. Copyright ©JOCSE, a supported publication of the Shodor Education Foundation Inc.

© 2020 Journal of Computational Science Education  
<https://doi.org/10.22369/issn.2153-4136/11/2/3>

## KEYWORDS

molecular dynamics, organic polymers, coarse-graining, magnetic-shape memory alloys, magnetic-shape memory, materials science, micropumps, BWSP

## 1 INTRODUCTION

MSM micropumps (Figure 1) represent a new paradigm of microfluidic mechanism, enabling accurate delivery of fluids over a wide range of densities and pressures [33]. MSM alloys including Ni-Mn-Ga enable such pumping through deformation under the influence of a magnetic field, which influences properties including twin motion deformation [38], strain [30], stress [29], magnetic and thermal activation [4, 38], operating temperatures [11, 35], magnetic permeability [22], and electric resistivity [32]. These properties make MSM alloys advantageous for use as actuators, channels, and pump membranes. In the case of MSM pumps, the aim is to exploit a localized constriction in the material (Figure 2) to encapsulate and propagate the working fluid against a sealant material as shown in Figures 2 and 3. Polydimethylsiloxane (PDMS) gel is a common sealant due to its low cost, bio-compatibility, moldability [8]. As the alloy is actuated it pulls away from the PDMS sealant, allowing fluid to be drawn in through the inlet port. Subsequently, as the fluid-filled constriction propagates toward the outlet due to the rotating magnetic field, the sealant re-adheres to the Ni-Mn-Ga surface, closing the inlet.

### 1.1 Simulations of Materials

The main focus of this manuscript is to advance understanding of PDMS/Ni-Mn-Ga interfaces by investigating the adhesion characteristics of the polymer sealant. Characterizing the nanoscale interface between PDMS and Ni-Mn-Ga (as seen in Figure 3) is challenging experimentally, so we use molecular simulations to explore PDMS/Ni-Mn-Ga adhesion. Molecular models for PDMS and Ni-Mn-Ga are individually available, but until this work no model exists that combines and describes interactions between both materials. Therefore, a focus of this work is creating this model.

A key component of the model is the “force field” defined by potential energy functions describing bonded and non-bonded interactions between each type of particle in the system. Bonded

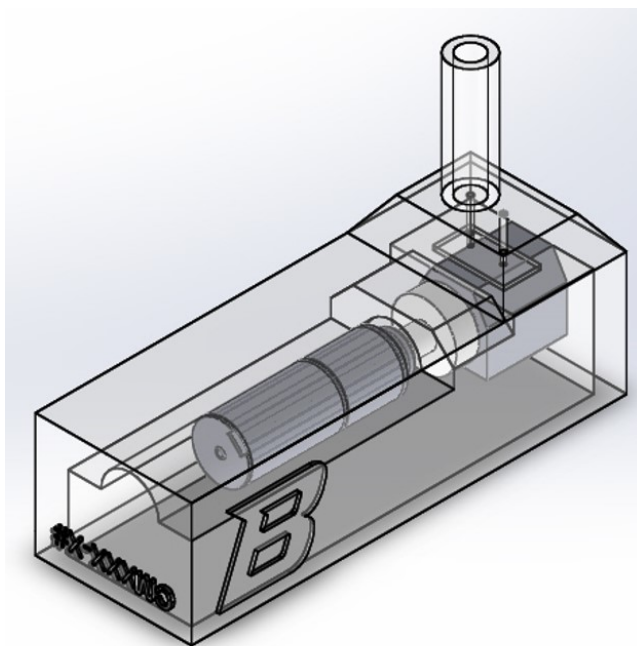


**Figure 1:** Model of a Ni-Mn-Ga micropump, showing placement of the MSM element, which is encapsulated in PDMS sealant, below the inlet/outlet reservoir.

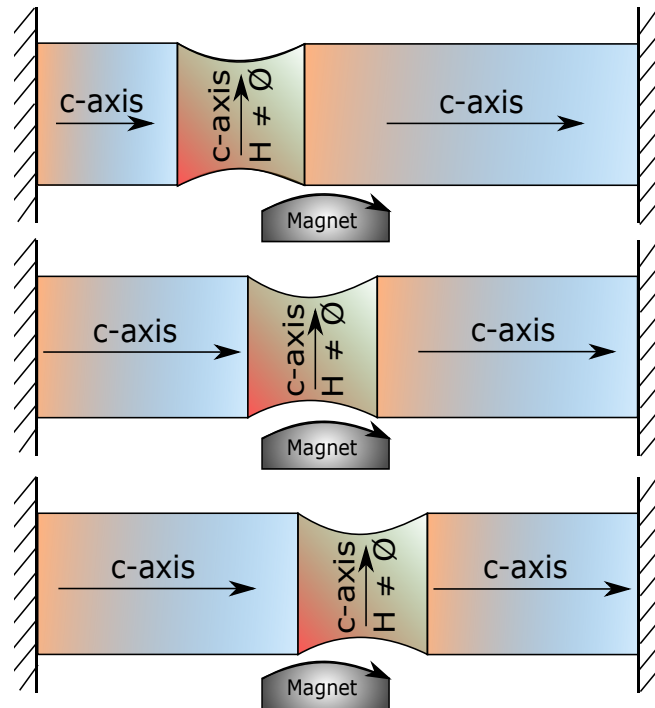


**Figure 2:** Three side views of the MSM micropump element illustrating the translation of the constriction along the *c*-axis as the magnetic field (*H*) is rotated. In a MSM pump, fluid is held between this constriction and the sealant material.

interactions are described as a set of constraints between bonded pairs (bond), triplets (angle) and quadruplets (dihedral) of particles that belong to the same molecule. Different forcefields vary in the functional forms used to model these constraints, so it is important to keep in mind any conversion factors when mapping from one forcefield to another and when combining multiple forcefields as we do here. Small differences in forcefield parameters can give rise to qualitatively different phase behavior and equilibrium structure [1].

We base our model on the Optimized Potentials for Liquid Simulations - United Atom model [21] (OPLS-UA) and UFF [5] force fields. There are several considerations to be made when constructing a new model. For instance, while some polymer models can describe how the conformation of a polymer chain evolves in a pristine thin film, varying the number of chains in the simulation, the average chain length, and polydispersity can strongly influence the interactions of the chains with themselves and other materials in the system [26]. Also, many alloy models are parameterized for a specific crystal structure and unit cell lattice parameters that are not necessarily transferable to other unit cells or crystallographic planes. Finally, it is important to ensure that the forcefields being combined are compatible with each other. As an example, the non-bonded Lennard-Jones interaction potentials used by Rappe *et al.* [5] in UFF are parameterized based on general hybridization rules, whereas Elliott and Akerson [7] rescale based on the bond dissociation energy, resulting in a thousand-times stronger interactions. While both approaches are self-consistent in that they correctly

describe the difference in interaction potentials between atoms defined within, naïvely combining the two would lead to the Elliott

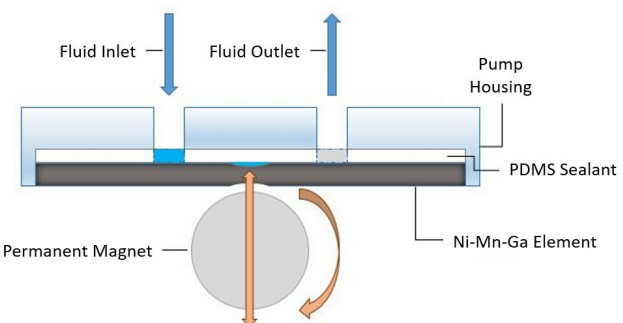


**Figure 3:** Schematic of a MSM pump interface showing the pocket of fluid bounded by the MSM and PDMS in transit from the inlet to outlet port of the pump.

forcefield dominating. Care must therefore be taken when combining interactions from different forcefields in the same simulation volume and so we iteratively test our model as we proceed and compare to observations in the literature to validate our work.

## 2 METHODS

We perform molecular dynamics (MD) simulations using HOOMD-Blue [2, 10] on NVIDIA Tesla K20X Graphic Processing Units (GPUs) at the Blue Waters supercomputer at the National Center for Supercomputing Applications [31] and P100 GPUs on our local cluster “Fry”.

### 2.1 Molecular Dynamics

MD simulations can efficiently sample the equilibrium structure of molecular systems by iteratively calculating the forces between neighboring particles and numerically updating positions using velocity and force information over discretized time steps. Here we employ the velocity-Verlet algorithm [1] and a tree-based neighbor list [15] that provides performance benefits for the non-isotropic systems studied here.

We perform MD simulations in the canonical (constant number of simulation elements  $N$ , volume  $V$ , and temperature  $T$ ) ensemble. The number of time steps to relax to equilibrium and to subsequently sample equilibrium microstates must be determined empirically as they depend on the forcefield, ensemble, and initial conditions. The initial configuration is specified with an XML file, which describes all of the particle properties including position, mass, atom type, charge, and velocity. The force field is then used to calculate the total force acting on each particle due to the interactions with their neighbors, which becomes an acceleration of the particle according to Newton’s second law of motion,  $F = ma$ , which in turn updates the velocity of the particle for the time step, which in turn updates the particle’s position. After particle positions are updated, these steps are repeated for each subsequent time steps. Individual microstates (specifying instantaneous positions and velocities) are written to a trajectory file (here, every 500 steps) as the simulation progresses. The trajectory is useful for visualizing system evolution and for post-processing material properties. Instantaneous potential energy and kinetic temperature measurements are recorded to quantify equilibration and check for unphysical behavior.

### 2.2 Computational Resources

The theoretical peak performance of K20X GPUs is 1.22 TeraFLOPS (or  $1.22 \times 10^{15}$  floating-point operations per second) for double (64-bit) precision performance and 2.9 TeraFLOPS for single (32-bit) precision performance. P100 GPUs have a peak performance of 4.7 TeraFLOPS for double-precision performance and 9.3 TeraFLOPS for single precision performance. When referring to the performance of these GPUs, double and single precision refers to the number of bits used to represent each floating point number used in the calculations. Generally, for these types of molecular simulations, single point float precision is sufficient for numerical stability without compromising computational efficiency [2]. Each MD simulation performed herein used a single CPU core driving a single

GPU, using Blue Waters’ K20X and Fry’s P100 hardware. Simulation benchmarking on both GPUs is presented in the Section 5.

## 3 MODEL

We specify the bonded and non-bonded PDMS interactions with the OPLS-UA force field. When running the surface interaction simulations with Ni-Mn-Ga we describe the polymer-surface interactions using UFF force field and polymer-polymer interactions with OPLS-UA. Surface-surface interactions are omitted from our investigation, and the Ni-Mn-Ga degrees of freedom are not integrated. This avoids modeling fast degrees of freedom of metallic bonds, which would require additional force fields such as the Embedded Atom Model [6] and more computational cost. Intrinsic to this constraint is the assumption that surface fluctuations are negligible on polymer fluctuation timescales. Here we describe the implementation details of the two material models individually and in combination.

### 3.1 Construction of PDMS

We construct PDMS topologies using the Avogadro [3] chemical drawing software. Using the tool, we draw the repeating monomer units (5 repeats shown in Figure 5), until reaching 20 (1.6 kDa), after which end caps (Figure 4 are added).

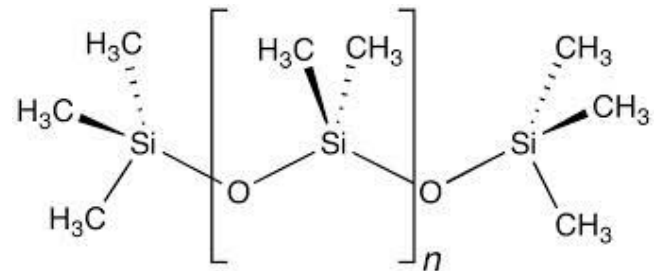


**Figure 4: Chemical formula for Polydimethylsiloxane (PDMS) [8].**

We then refine the 20-mer model from above in Jupyter notebook [24] that utilize mBuild [23] and Foyer [17], toolkits for managing molecule creation and forcefields. In Figure 5 and Figure 6 each sphere represents one United Atom (UA) simulation element. Each UA simulation element represents a “heavy” atom such as Carbon, Oxygen, or Silicon and its associated Hydrogens. This simplification accelerates sampling of the molecular dynamics without sacrificing structural accuracy [12, 27, 28].

PDMS has been studied extensively in the literature, and there is a wealth of information on possible simulation forcefields. For this investigation, we describe the non-bonded inter-molecular, and bonded intra-molecular interactions of PDMS using parameters obtained from the works of Frischknecht and Curro [9] and Tamai *et al* [36]. The complete set of parameters is given in Table 1.

The bonded interaction parameters are described as parameterizations of the following equations [9]:

$$V_b(r) = k_b(r - r_0)^2 \quad (1)$$

$$V_a(\theta) = k_\theta(\theta - \theta_0)^2 \quad (2)$$

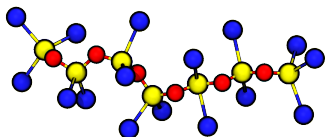


**Figure 5:** 5-mer chain of PDMS built using a Jupyter notebook, with energy minimized through Avogadro [3], and visualized with VMD [16]

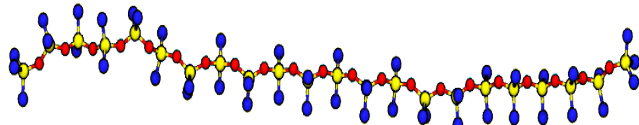


**Figure 6:** 20-mer chain of PDMS visualized with VMD [16]

$$V_t(\phi) = k_t [1 + \cos(n\phi)] \quad \text{and} \quad \phi = \pi \quad (3)$$

where  $V_b$ ,  $V_a$ , and  $V_t$  describe the pairwise bond, triplet angle, and quadruplet dihedral potentials, and are functions of separation,  $r$ , in-plane angle,  $\theta$ , and out-of-plane angle,  $\phi$ , respectively. These potentials are dependent on the constraint coefficients  $k_b$ ,  $k_\theta$ , and  $k_t$ , which are taken from the work of Frischknecht and Curro.

The non-bonded pairwise interactions were taken from Tamai *et al.*, describing the balance between short-range atomic repulsion and long-range Van der Waals attraction as a Lennard-Jones potential:

$$V(r) = -4\epsilon \left( \left( \frac{\sigma}{r} \right)^{12} - \left( \frac{\sigma}{r} \right)^6 \right), \quad (4)$$

where  $\sigma$  and  $\epsilon$  control the shape of the interaction at varying separation  $r$ , and are dependent on the types of atoms in the pair being considered.

bonds	$r_o[\text{\AA}]$	$k_b [\text{kJ}/(\text{mol nm}^2)]$
Si-O	1.647	146490.2
Si-CH <sub>3</sub>	1.866	79337.0
angles	$\theta_o[\text{rad}]$	$k_\theta [\text{kJ}/(\text{mol rad}^2)]$
Si-O-Si	2.547	59.162
O-Si-O	2.076	395.388
CH <sub>3</sub> -Si-CH <sub>3</sub>	1.844	209.074
O-Si-CH <sub>3</sub>	1.875	209.074
dihedrals	$n$	$k_t [\text{kJ/mol}]$
Si-O-Si-O	1	1.8828
Si-O-Si-CH <sub>3</sub>	3	0.083638
nonbonded	$\sigma [\text{\AA}]$	$\epsilon [\text{kJ/mol}]$
Si	3.385	2.4480
O	2.955	0.8493
CH <sub>3</sub>	3.786	0.7532
Ni	2.522	0.2510
Mn	2.635	0.2176
Ga	3.901	6.9454

**Table 1:** Potential Parameters for PDMS and Ni-Mn-Ga [5, 9, 36]

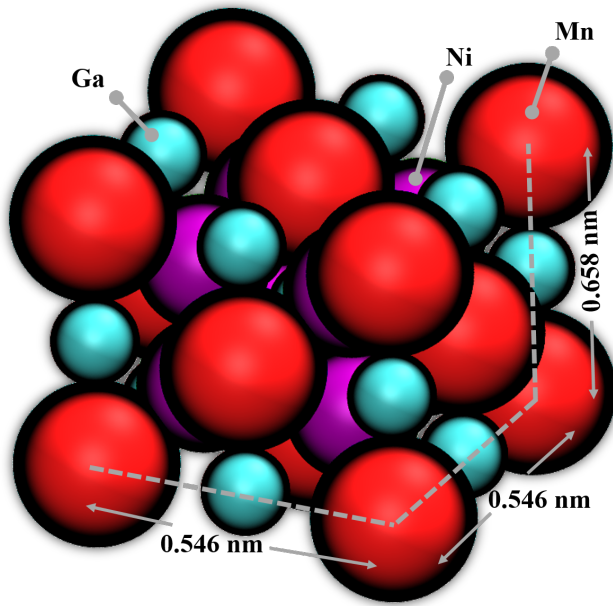


**Figure 7:** Unit cell of Ni-Mn-Ga with lattice parameters for a Non-Modulated (NM) crystal, visualized using VMD [16]

As per the molecular dynamics algorithm, interaction forces are calculated at each discrete time step ( $\delta t$ ). For our initial PDMS simulations, we use  $\delta t = 0.001$  fs. After calibrating our model, we found we could increase this time step without resulting in numerical inconsistencies. Therefore, for the final PDMS simulation and for all the interface simulations, we use  $\delta t = 1$  fs. The increase in simulation time step is beneficial as it permits a longer period of material simulation per minute of elapsed “wall-clock” time.

### 3.2 Construction of Ni-Mn-Ga

We use Avogadro [3] to construct the Ni-Mn-Ga surface, as it includes crystallography tools to position the atoms of the unit cell. We employ lattice constants

$$a = b = 0.546 \text{ nm}$$

$$c = 0.658 \text{ nm}.$$

as specified in Sozinov *et al.* [34].

The atomic coordinates themselves are taken from Hickel *et al.* [13]. The resulting unit cell of Ni-Mn-Ga, as shown in Figure 7, is then used as a building block for surfaces of varying sizes based on arranging multiple cells in a lattice, the size of which can be easily tuned as an input.

We employ UFF developed by Rappé *et al* [5] to provide interaction parameters for PDMS with Ni-Mn-Ga. However, because UFF lacks bonded constraint parameterizations for PDMS we must simultaneously employ OPLS-UA and UFF to simultaneously model surface-PDMS and PDMS-PDMS interactions. This is the first work to our knowledge to combine these force fields to investigate PDMS on Ni-Mn-Ga. The complete list of nonbonded interaction parameters for Ni-Mn-Ga used in our investigation can be found in Table 1.

## 4 DATA WORKFLOWS

Key open-source software packages used in this work include: mBuild [23], Foyer [17], MorphCT [18, 20], and Rhaco [19]. mBuild and Foyer are MD toolkits developed by the Molecular Simulation Design Framework team, aiding molecule building and atom typing, respectively, used here to create XML files input into HOOMD. MorphCT and Rhaco are used for checking periodic particle image information and initializing molecules on surfaces. As part of this work, Rhaco was generalized in order to accept a Ni-Mn-Ga unit cell as the surface template allowing us to initialize PDMS in its vicinity and to control the MD simulation of these two materials.

Therefore, the key contributions of this paper are the following:

- **MSM–Polymer Simulations -**

These are the first MD simulation of Ni-Mn-Ga with PDMS. This work also differs from prior MSM work that focuses on twin boundary movement within the alloy and the mechanisms by which this occurs. This paper reports the simulated interactions of this alloy with PDMS.

- **Educational Value (J.Guevara) -**

Working on this project has exposed me to many areas of both research and Computational Science, from learning how to gather the necessary data to begin simulations, to knowing how to collaborate with others. I gained significant experience in how to use Python for scripting, programming, and statistical analysis, as well as significant knowledge on the interaction of organic polymer and metal interfaces from a molecular standpoint. Furthermore, this experience has made me want to continue to pursue, and learn more about, High Performance Computing.

## 5 RESULTS

### 5.1 Performance

Initial PDMS simulations containing 7,120 particles took 45 minutes to complete  $10^7$  time steps on Blue Waters XK nodes (over 3,700 time steps per second (TPS)). These simulations informed additional, larger simulations on P100 GPUs on Fry. With P100 cards, we perform simulations of 36,900 particles at 3,600 TPS – a factor of 5 increase in system size with similar run time. In total, we submitted 60 pure (“neat”) PDMS jobs (25 on Blue Waters and 35 on Fry) and 14 jobs with PDMS/Ni-Mn-Ga interfaces (all on Fry) for a total of 33 hours and 14 minutes of wall clock time for simulations with analyzable trajectories. We estimate many hundreds of unsuccessful simulation jobs were submitted (unphysical initial conditions,  $\delta t$  too large, missing packages in the software stack, etc.).

### 5.2 Neat PDMS

Neat PDMS systems containing 80 20-mer chains (7,120 particles) are simulated using HOOMD for  $10^5$  time steps at a temperature of  $T = 294$  K. However, for transferability of simulations and numerical accuracy, HOOMD records the temperature in reduced units,  $T^*$ , based on a reduced energy scaling parameter,  $\epsilon$ . For the initial PDMS volumes  $\epsilon = 0.585$  kcal/mol. The following equation can be used to map between the real and dimensionless temperatures:

$$T^* = \frac{k_B T}{\epsilon}, \quad (5)$$

where  $k_B$  is Boltzmann’s constant. We encountered some issues simulating our initial PDMS volumes, which are detailed in Section 7.1.

Figure 8 shows the simulation temperature, nonbonded potential energy, and total potential energy for our PDMS system after fixing issues corresponding to volume packing, image, and interaction parameter corrections. The kinetic temperature (8a) equilibrates quickly, with non-periodic temperature fluctuations of around 20–30K. Additionally, the potential energies presented in 8b and c exhibit a roughly-exponential relaxation as molecules reorganize into free energy minimizing configurations, followed by a period of constant average energy signifying equilibration of the system.

Another useful tool for analyzing the output of our simulation is the visualization software VMD (Visual Molecular Dynamics) [16]. VMD allows us to view the trajectories, helping to understand how the system evolves over time and what the final relaxed systems looks like. Visualizing the final trajectory can provide useful insights into any issues with the initialization of our simulations, or any bugs in the code, as described in Section 7.1.

### 5.3 PDMS with Ni-Mn-Ga Surface

Several issues needed to be addressed before equilibrated PDMS on Ni-Mn-Ga configurations could be sampled (Section 7.1). After fixing these bugs, we perform simulations of 100 PDMS chains in the presence of a 20x20x1 unit cell Ni-Mn-Ga slab at 294K. These simulations took around 40 seconds to simulate  $10^4$  time steps, and around 45 minutes to simulate  $10^7$  time steps – a similar wall-clock time to those noted in our initial neat PDMS tests. The resultant simulation trajectories after are shown in Figure 9. We also present the temperature and potential energy evolution of the simulations in Figure 10, demonstrating the small non-periodic fluctuations in both, and the eventual equilibration of the system according to the potential energy. That the kinetic temperature, nonbonded, and total energies all independently stabilize after  $\approx 2$  ns supports our interpretation that these systems reach equilibrium (or at least a metastable state). The PDMS is observed to quickly aggregate (within the first 50 frames of our visualization) and then sticks to the surface to form a film over the alloy layer.

To test our simulation model and Rhaco further, we simulate the same system at a higher temperature: 500 K (approx. 227°C). The increased thermal energy should translate to an increase in the speed at which the PDMS atoms move. Additionally, since the boiling point of PDMS is around 473 K, we would expect the vaporization of the polymer, leading to it filling the simulation volume rather than forming a liquid film at the alloy surface. Indeed, the visualization of the simulation shows the molecules interacting faster with each other, and Figure 11 shows the PDMS filling the simulation volume and adhering less to the alloy at 500 K compared to 294 K. Figure 11 also shows a rather visually drastic change in the PDMS, however the chains do stick together and seem far more drastic since we are compressing  $10^5$  –  $10^7$  timesteps into a much shorter 500 simulation frames during visualization. Figure 12 shows the equilibration of the temperature and potential energy of the high-temperature system. Note that the fluctuations are larger and the system equilibrates sooner than in the liquid case at 294 K.

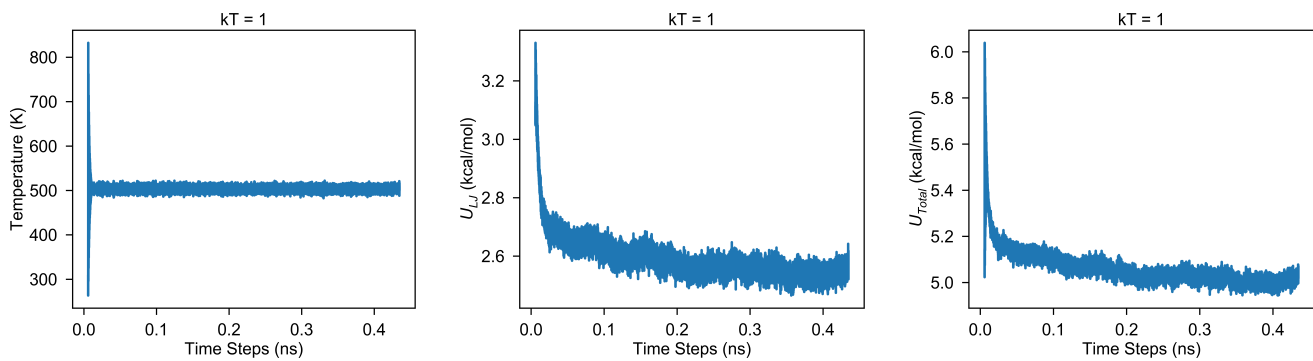


**Figure 8:** Energy profiles for an 80 20-mer volume of PDMS, for the same simulation temperature,  $k_B T = 1$ , approximately 500 K. Potential energies (both Lennard-Jones and total) are per mole.

## 6 DISCUSSION

The final model presented here permits the equilibration and sampling of PDMS on Ni-Mn-Ga efficiently across a range of state points. Identifying this model required iterative testing checking for artefacts including periodic oscillation of temperature, or inaccurate combinations of forcefields. Early test showed that PDMS did not adhere as the sealant on the alloy, instead aggregating away from the surface (Section 7.1). The final model instead shows the

two materials to attract and permits surface structure to be investigated, therefore providing a starting point for understanding the sealant-alloy interface.

We now turn to comparing our simulation results to literature, in order to validate our model's accuracy. While there are not to our knowledge experimental values of PDMS and Ni-Mn-Ga surface energies to compare against there have been molecular investigations with PDMS interacting with other materials. Comparisons of molar energies and surface energies with such studies, despite their differences, provide useful benchmarks for future improvements to the present work. For instance, the work of *Liu et al.* [25] shows the MD simulation of PDMS interacting with a Zeolite (ZSM-5) surface using the COMPASS force field. We note that ZSM-5's structure is dissimilar to Ni-Mn-Ga, however we are interested in the fact that this is an MD simulation of PDMS with another material for which energy values are provided in a manner that we can easily calculate and compare to ours. In the manuscript, the authors report the total nonbonded interaction energy of PDMS as being -1885.6 kcal/mol. This interaction energy is a total energy of the system as a whole, in contrast to the energies per mole reported in Figures 10 and 12. Reporting energies per mole allows for a direct comparison between the 7,120 particle PDMS-only simulations and the 21,700 particle combined PDMS Ni-Mn-Ga simulations. The simulations in *Liu et al.* contain five chains, each made up of four repeating units, which we calculate to contain 235 total atoms in the system. The per-atom PDMS nonbonded potential energy from *Liu et al.* is therefore 8.02 kcal/mol, which is in good agreement with our simulated value of 2.6 kcal/mol for our simulated volume of PDMS by being within the same order of magnitude. We would not expect our non-bonded values to align perfectly, given that the biggest difference in simulation is the simulation temperatures: 303K for *Liu et al.* vs. 500K for ours. We can perform similar analysis for the PDMS-Zeolite simulations, according to the reported total nonbonded potential energy of -13073.4 kcal/mol. Using the same number of atoms, and an estimated 288 atoms present in the authors' Zeolite unit cell, we obtain a per-atom nonbonded PDMS-Zeolite potential energy of 25.00 kcal/mol, which is within a factor of two of the 14.62 kcal/mol energy calculated from our simulations. We also note a consistent ratio between the neat PDMS interaction

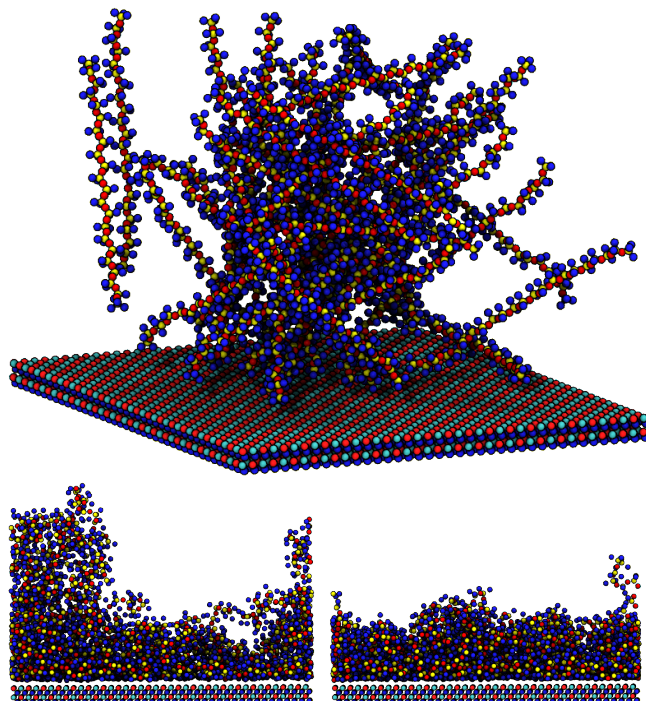


**Figure 9:** First time step (top) and the contrast of the 20<sup>th</sup> time step (bottom-left) and the last time step (bottom-right), of our interface.

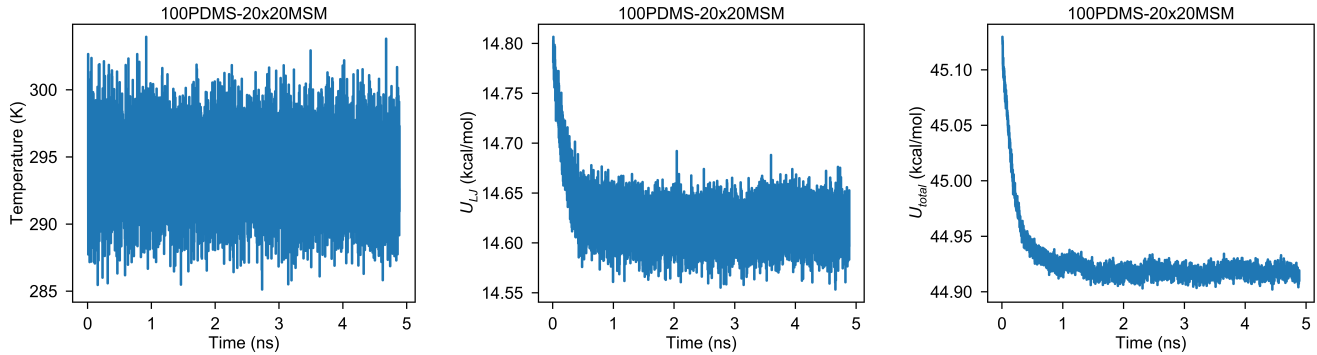


**Figure 10:** Energy profiles for our Ni-Mn-Ga–PDMS interface at a set simulation temperature of 294K. Both potential energies, Lennard-Jones and total, are per mole.

energies and the surface energies in our work compared to *Liu et al.* The ratio of PDMS-Ni-Mn-Ga interaction energies to neat PDMS is 5.6. Similarly, the ratio between PDMS-Zeolite interaction energies and neat PDMS in *Liu et al.* is 3.1. The similarity and order-of-magnitude quantitative agreement in these calculated energy levels lends additional confidence to our hybrid OPLS-UA/UFF forcefield, while providing additional versatility over COMPASS by parameterizing interactions between any elemental atoms in the periodic table. Furthermore, it must be noted that the substrates in the simulations of *Liu et al.* and ours, Zeolite and Ni-Mn-Ga respectively, are dissimilar which is why despite the energy ratios not being the same, the fact that they're within an order of magnitude gives us confidence that our model is within the realm of credibility. This

is not to say that the model cannot be more finely tuned to more closely yield results to those of *Liu et al.*, but rather that by being within such a factor and order of magnitude our simulation does not, at this current first glance, require more than some parameter modifications as opposed to a full rebuild. *Tsige et al.* [37] present a similar simulation of neat PDMS, containing 100 20-mers of the elastomer with SiO<sub>2</sub>. This simulation is important, not because of the substrate, but rather because the PDMS used in this simulation covers the exact same chain length and number of chains as our simulation, making it another great point of reference. The authors report a nonbonded potential energy of 6 kcal/mol at a separation of 4 Å, in good agreement with the current model. This is to say that this reported value lies within the range of nonbonded values that we see in our model: 2.6 kcal/mol for PDMS by itself and 14.62 kcal/mol for PDMS–Ni-Mn-Ga, where our metal substrate has more of an influence than SiO<sub>2</sub>.

Being able to simulate PDMS and Ni-Mn-Ga together opens up significant opportunities for future study, from both HPC and materials science perspectives. We can continue to hone our toolkits and algorithms to yield more efficient and accurate simulations, reducing computational cost while maintaining good quantitative agreement with experiment. From a materials viewpoint, the model demonstrated here provides an excellent staging ground for understanding surface-sealant interactions for micro-electro-mechanical systems, guiding manufacturing processes and focussing future experimentation efforts.

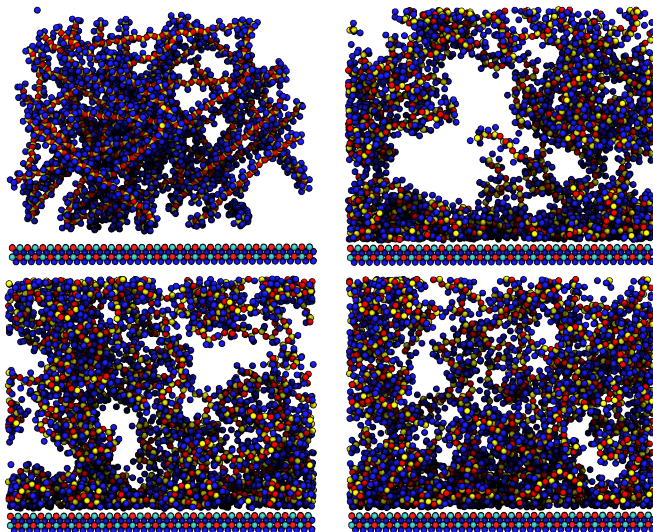


**Figure 11:** Progression of our interface model at a temperature of 500 K. First frame (top-left), 100<sup>th</sup> frame (top-right), 250<sup>th</sup> frame (bottom-left), and final frame (bottom-right). We observe PDMS self-aggregating at less 500 K than at 294 K (Fig. 9), as expected.

## 7 INTERNSHIP REFLECTION

To meet the JOCSE aim of improving computational science education, we reflect on pivotal learning moments over the course of the Blue Waters Student Internship Program (BWSIP).

A problem that can arise through these simulations comes when particles are too tightly bound within a simulation space. If the user doesn't take care in adjusting time steps and integrator time constants to control thermostating, numerical instabilities can result in unphysical particle displacements (sometimes referred to as the simulation “exploding”).

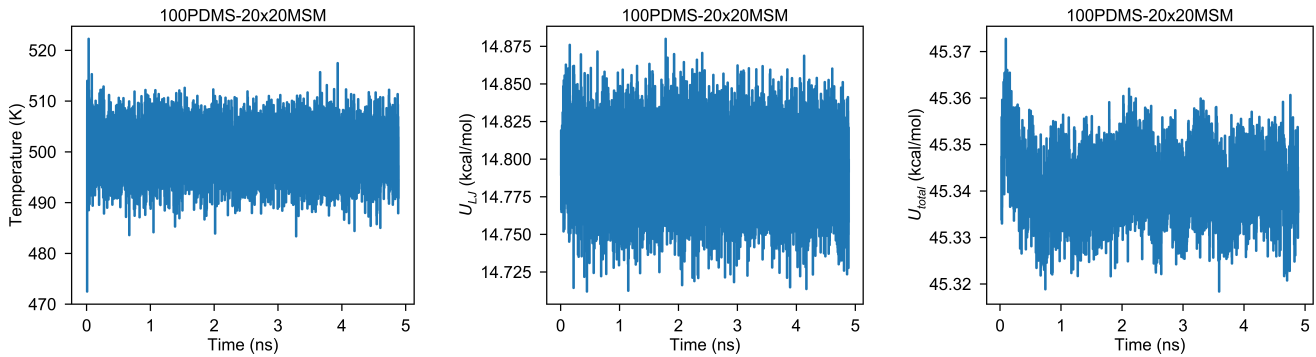


**Figure 12:** Energy profiles for our Ni-Mn-Ga–PDMS interface at a set simulation temperature of 500K. Both potential energies, Lennard-Jones and total, are per mole.

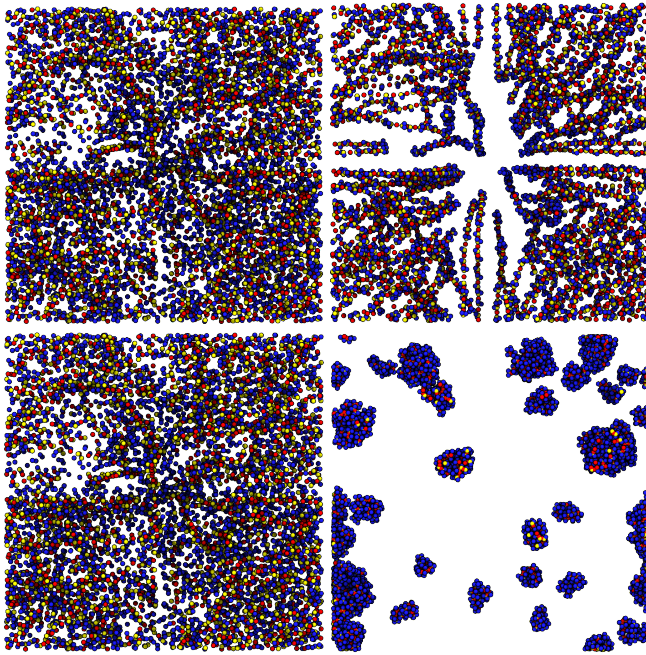


**Figure 13:** Larger time steps advance simulations faster. (top row) After the first time step  $\delta t = 10^{-3}$  fs (left) and  $\delta t = 1$  fs (right). (bottom row) final snapshots after  $10^3$  steps.

## 7.1 Troubleshooting

After the two basic structures for our PDMS molecule, and our Ni-Mn-Ga alloy, were finished they were then put into simulations. Previously, it was mentioned that PDMS was chosen to be constructed first, as it would allow for better early testing. This testing was not only meant to be of the material, but also of the code we wrote to initialize and perform these simulations. Over the course of the last year many issues were resolved with the PDMS simulations, the biggest of these problems being the following:

**7.1.1 Timestep Selection.** In Figure 13 we can see a problem resulting when the time step is too small. The snapshots in the left

column show after the 1st (top) and 1000th (bottom) step when  $\delta t = 0.001$  fs. The snapshots in the right column show after the 1st (top) and 1000th (bottom) step when  $\delta t = 1$  fs. Even after the first snapshot there is a visible difference between the 0.001 fs and 1 fs cases, and after 1000 steps the 1 fs case shows PDMS aggregating while the 0.001 fs case has now changed. Here, a step size of 0.001 fs is so small that position changes fall below the rounding threshold in 32-bit precision addition during integration, and the system is essentially frozen. Visualizing the trajectory quickly identifies this problem, but such a problem may go undetected if not visualized because the 0.001 fs system is numerically stable and quickly “equilibrates”.

**7.1.2 Image Correction.** To enable a finite number of particles to represent bulk interfacial areas, periodic boundary conditions are employed. These boundaries are not boundaries: when a simulation element moves out of the left-hand face of the box, it enters again from the right, and particle interactions are considered across periodic boundaries along each axis. HOOMD therefore needs to keep track of which periodic image that the particle is in, in order to calculate how far it has traveled in the system. Initially, every particle in the system is located in the original simulation volume and has image indices [0, 0, 0]. However, our initial XML files did not contain these indices even after we had established the other parameters in our XML, leading to numerical instabilities in our simulation. This problem was solved through by using MorphCT to manipulate our initial XML file to obtain the correct formatting for HOOMD.

**7.1.3 Coefficient Correction.** When trying to simulate a larger volume of PDMS from the molecules we first produced, an error with the bond, angle, and dihedral coefficients was encountered: They were missing from the XML file. Without these coefficients, the conformational structure of PDMS could not be maintained and the atoms in the molecules would act as if they were not bonded to anything. This would undoubtedly lead to incorrect particle trajectories and unreliable results about the interaction of PDMS with the Ni-Mn-Ga surface. This problem was solved by using mBuild’s builder package to populate the bond, angle, and dihedral coefficients accordingly based on a neighbor list it created for each

of the particles present in the system. Furthermore, we also needed to rescale the system in order to correct incorrect, and inconsistent, distances along with the energy that the system takes in from the forcefield used.

In the initial surface simulations, we noticed very strong polymer-polymer interactions but significantly weaker polymer-surface adsorption as shown in Figure 14. At first this was attributed to PDMS desorbing over long timescales. Further investigation revealed that a UFF unit conversion problem resulting in negligible interactions between the PDMS and the Ni-Mn-Ga. Reworking the potential parameters to the units Rhaco expected resolved this issue: After the OPLS-UA and UFF potentials were calibrated, PDMS integrated was successful and adsorption onto Ni-Mn-Ga was observed.

**7.1.4 Volume Packing.** This problem presented early on when trying to produce a sample volume of PDMS where the number of molecules being packed into our early systems exceeded the size of the system itself. This then would continuously lead to our simulations “exploding” - a colloquial term used when atoms are placed so close to each other that they experience strong repulsion from the Lennard-Jones equation, often many orders of magnitude greater than the forces expected throughout the rest of the system. The large forces lead to large velocities of particles, and in a single time step an atom can move distances many times larger than the simulation volume, causing the program to crash. This issue was resolved by changing our input of molecules by using an reduced number, this then let mBuild pack our molecules at a lower density than the physical material.

**7.1.5 Integrator ringing.** The evolution of the system temperature in Figure 15 for this initial simulation shows that the simulation needs to run for at least 100,000 time steps in order for it to stabilize around the set point. Additionally, periodic “ringing” of the temperature can be observed, as the thermal energy of the system oscillates around the set point. HOOMD regulates its temperature through the use of the Nosé-Hoover thermostat [14], which couples to an infinite thermal bath and injects (removes) thermal energy to (from) the simulation by increasing (decreasing) the velocities of the atoms in the simulation, regulating its temperature. The strength of this coupling can be modified using the parameter  $\tau$ . Selecting an

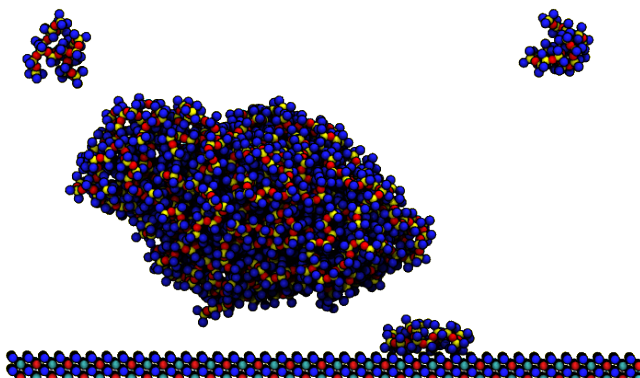


Figure 14: End state of initial testing of PDMS and Ni-Mn-Ga through the use of Rhaco

appropriate  $\tau$  is extremely important to avoid unphysical ringing from the integrator. If  $\tau$  is too high, then the timescale of energy control is large and initial deviations from the set point may take millions of steps before stabilizing. If  $\tau$  is too low it permits the integrator to “overshoot” the set point, and the ringing seen above occurs as the integrator iteratively removes and adds kinetic energy over short times, oscillating about the setpoint. Periodic oscillations of the temperature are indicative of an unbalanced  $\tau$  value, and it is important to modify tau incrementally to obtain consistent, random fluctuations around the set point temperature.

In addition to having a stable temperature, the stability of the potential energy of the system is also important for molecular dynamics simulations. As the molecules relax in the system, the potential energy decreases as the simulation attempts to find the global minimum of free energy (balancing potential energy minimization with entropy maximization and therefore the most likely conformations of molecules thermodynamically). When the potential energy no longer evolves, the equilibrium energy has been found. Generally, small systems and those at high temperature equilibrate quickly, whereas larger systems or those at low temperature can take millions of time steps for the potential energy to stop evolving. It is therefore imperative to consider both the

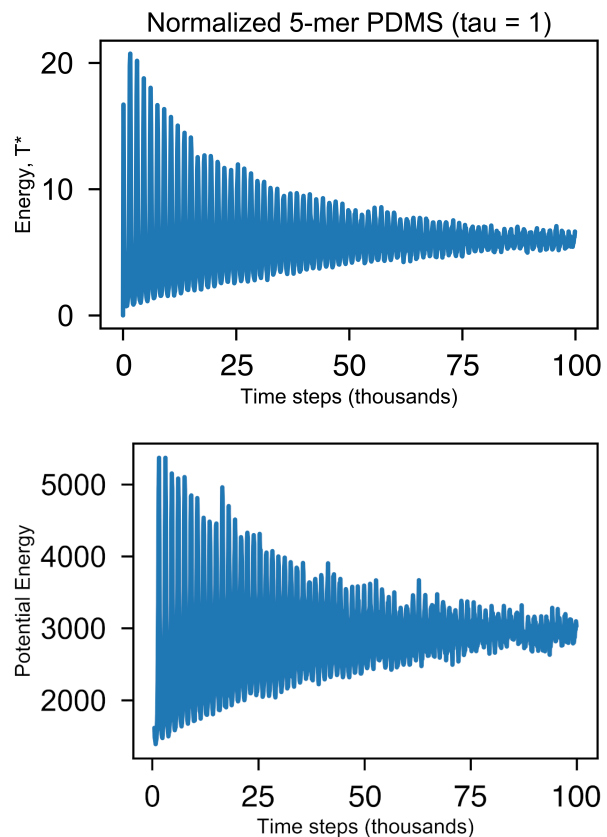
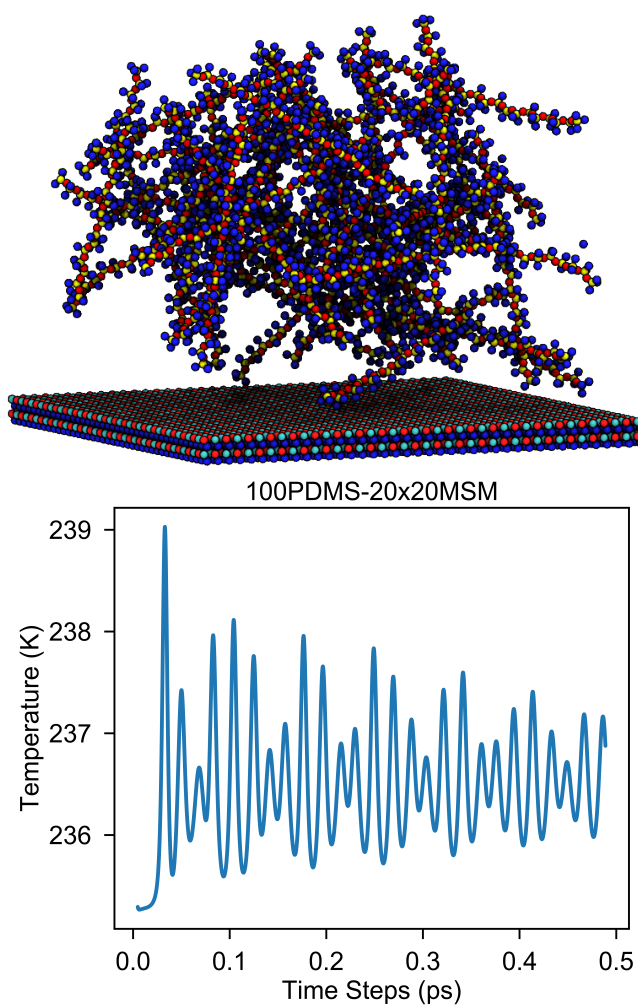


Figure 15: Energy plots for our initial 5-mer chain. Temperature/Kinetic (top), and Potential (bottom)

temperature and the potential energy before reporting structural or energetic results for a molecular dynamics simulation.

As an example, initial simulations of the PDMS and alloy yielded some promising results, as shown in Figure 16 for a system of 36,100 particles. However, the temperature profile of the simulation also demonstrates integrator ringing. This indicates that the value of  $\tau$  is unbalanced, and could also suggest that longer runtimes are needed for this simulation. In fact, on further review, these data identified a critical bug in Rhaco. While Rhaco was successfully able to generate the interface observed in Figures 16 and 14, the conversion calculation between the dimensionless simulation temperature and the real temperature in Kelvin was incorrect and needed to be fixed. This error arose from the surface atoms being assigned initial velocities, even though those atoms were omitted from the integrator and never actually moved in the simulation. The additional kinetic energy in the system was interpreted as an increased temperature, offsetting our reported temperatures by several hundreds of Kelvin.



**Figure 16: Initial testing of the PDMS-Ni-Mn-Ga interface showing some attempt at temperature stabilization.**

## 8 CONCLUSIONS

While being able to fully simulate the interaction of PDMS and Ni-Mn-Ga alloy inside of a microfluidic pump is a significant challenge, we here demonstrate the first steps towards achieving that goal. We develop and present a successful model and toolkit for simulating the interactions of the sealant at an alloy surface. Our model is versatile in terms of input parameters, allowing us to test systems of different sizes, PDMS densities, alloy thickness, and processing temperatures, and can be easily extended to include additional materials such as solvents and dyes in the simulation volume. For the future we hope to develop additional analysis tools that can calculate surface energies more rigorously, include additional infrastructure to simulate twin-boundary dislocations in the alloy and ascertain the effect this has on the PDMS adsorption, as well as identify other, superior sealant candidates for this application. Pedagogically, this has been a great introduction into High Performance Computing (HPC) and computation in general, especially in how to best optimize code: The original simulation code took 40-45 minutes to produce a trajectory for a relatively small amount of neat PDMS, whereas the final tool could simulate the interactions large amounts of both PDMS and Ni-Mn-Ga alloy in approximately the same wall-clock time, representing a simulation time of several nanoseconds. Although my allocation on Blue Waters has come to an end for this project, the lessons learned over my time working with this system will definitely aid JG in the future, be it in continuing with this work, testing different versions of this interface, or with HPC as a whole.

## 9 ACKNOWLEDGEMENTS

This work was supported by a grant from the Shodor Education Foundation through the Blue Waters Student Internship Program (BWSIP) and by the National Center for Supercomputing Applications, who provided hardware used in this project. National Science Foundation through project NSF-DMR 1710640. This work used the computing resources supported by Boise State College of Engineering Information Technology services.

## REFERENCES

- [1] Mp Allen. 2004. Introduction to Molecular Dynamics Simulation. *Comput. Soft Matter From Synth. Polym. to ...* 23, 2 (2004), 1–28. <http://citeseerx.ist.psu.edu/viewdoc/download?doi=10.1.1.93.3254&rep=rep1&type=pdf%5Cnhttp://dasher.wustl.edu/chem478/reading/md-intro-2.pdf>
- [2] Joshua A. Anderson, Chris D. Lorenz, and A. Travesset. 2008. General Purpose Molecular Dynamics Simulations Fully Implemented on Graphics Processing Units. *J. Comput. Phys.* 227, 10 (may 2008), 5342–5359. <https://doi.org/10.1016/j.jcp.2008.01.047>
- [3] Avogadro. 2012. An open-source molecular builder and visualization tool. Version 1.2.0. <http://avogadro.openmolecules.net/>
- [4] V. A. Chernenko, V. L'vov, J. Pons, and E. Cesarri. 2003. Superelasticity in high-temperature Ni-Mn-Ga alloys. *J. Appl. Phys.* 93, 5 (2003), 2394–2399. <https://doi.org/10.1063/1.1539532>
- [5] K. S. Colwell, C. J. Casewit, W. A. Goddard, W. M. Skiff, A. K. Rappe, C. J. Casewit, K. S. Colwell, W. A. Goddard, and W. M. Skiff. 2005. UFF, a full periodic table force field for molecular mechanics and molecular dynamics simulations. *J. Am. Chem. Soc.* 114, 25 (dec 2005), 10024–10035. <https://doi.org/10.1021/ja00051a040> arXiv:1305.7119
- [6] Murray S. Daw and M. I. Baskes. 1984. Embedded-atom method: Derivation and application to impurities, surfaces, and other defects in metals. *Phys. Rev. B* 29, 12 (1984), 6443–6453. <https://doi.org/10.1103/PhysRevB.29.6443>
- [7] Ryan S. Elliott. 2018. Efficient ‘Universal’ Shifted Lennard-Jones Model for All KIM API Supported Species Developed by Elliott and Akerson (2015) v003. <https://doi.org/10.25950/962b4967>
- [8] Elveflow. 2005. PDMS: A Review. <https://www.elveflow.com/>

- [9] Amalie L. Frischknecht and John G. Curro. 2003. Improved United Atom Force Field for Poly(dimethylsiloxane). *Macromolecules* 36, 6 (mar 2003), 2122–2129. <https://doi.org/10.1021/ma025763g>
- [10] Jens Glaser, Trung Dac Nguyen, Joshua A. Anderson, Pak Lui, Filippo Spiga, Jaime A. Millan, David C. Morse, and Sharon C. Glotzer. 2014. Strong Scaling of General-purpose Molecular Dynamics Simulations on GPUs. *Comput. Phys. Commun.* 192 (dec 2014), 97–107. <https://doi.org/10.1016/j.cpc.2015.02.028> arXiv:1412.3387
- [11] Oleg Heczko and Ladislav Straka. 2003. Temperature dependence and temperature limits of magnetic shape memory effect. *J. Appl. Phys.* 94, 11 (2003), 7139–7143. <https://doi.org/10.1063/1.1626800>
- [12] Michael M Henry, Matthew Lewis Jones, Stefan D Oosterhout, Wade A Braunecker, Travis W Kemper, Ross E Larsen, Nikos Kopidakis, Michael F Toney, Dana C Olson, and Eric Jankowski. 2017. Simplified Models for Accelerated Structural Prediction of Conjugated Semiconducting Polymers. *J. Phys. Chem. C* 121, 47 (nov 2017), 26528–26538. <https://doi.org/10.1021/acs.jpcc.7b09701>
- [13] Tilman Hückel, Matthé Uyttewaal, Ali Al-Zubi, Biswanath Dutta, Blazej Grabowski, and Jörg Neugebauer. 2012. Ab Initio-Based Prediction of Phase Diagrams: Application to Magnetic Shape Memory Alloys. *Adv. Eng. Mater.* 14, 8 (aug 2012), 547–561. <https://doi.org/10.1002/adem.201200092>
- [14] William G. Hoover. 1985. Canonical Dynamics: Equilibrium Phase-space Distributions. *Phys. Rev. A* 31, 3 (1985), 1695–1697. <https://doi.org/10.1103/PhysRevA.31.1695>
- [15] Michael P. Howard, Joshua A. Anderson, Arash Nikoubashman, Sharon C. Glotzer, and Athanassios Z. Panagiotopoulos. 2016. Efficient Neighbor List Calculation for Molecular Simulation of Colloidal Systems Using Graphics Processing Units. *Comput. Phys. Commun.* 203 (2016), 45–52. <https://doi.org/10.1016/j.cpc.2016.02.003>
- [16] William Humphrey, Andrew Dalke, and Klaus Schulten. 1996. VMD: Visual molecular dynamics. *J. Mol. Graph.* 14, 1 (feb 1996), 33–38. [https://doi.org/10.1026/0263-7855\(96\)00018-5](https://doi.org/10.1026/0263-7855(96)00018-5)
- [17] Christopher R Iacobella, Janos Sallai, Christoph Klein, and Tengyu Ma. 2017. Idea Paper: Development of a Software Framework for Formalizing Forcefield Atom-Typing for Molecular Simulation. <https://github.com/mosdef-hub/oyer>.
- [18] M. L. Jones. 2018. MorphCT - DOI: 10.5281/zenodo.1243843. <https://doi.org/10.5281/zenodo.1243843>
- [19] M. L. Jones. 2018. Rhaco - DOI: 10.5281/zenodo.1308187. <https://doi.org/10.5281/zenodo.1308187>
- [20] Matthew Lewis Jones and Eric Jankowski. 2017. Computationally connecting organic photovoltaic performance to atomistic arrangements and bulk morphology. *Mol. Simul.* 43, 10-11 (mar 2017), 1–18. <https://doi.org/10.1080/08927022.2017.1296958>
- [21] William L. Jorgensen and Julian. Tirado-Rives. 1988. The OPLS [Optimized Potentials for Liquid Simulations] Potential Functions for Proteins, Energy Minimizations for Crystals of Cyclic Peptides and Crambin. *J. Am. Chem. Soc.* 110, 6 (mar 1988), 1657–1666. <https://doi.org/10.1021/ja00214a001>
- [22] D. Kikuchi, T. Kanomata, Y. Yamaguchi, H. Nishihara, K. Koyama, and K. Watanabe. 2004. Magnetic properties of ferromagnetic shape memory alloys Ni<sub>2</sub>Mn<sub>1-x</sub>Fe<sub>x</sub>Ga. *J. Alloys Compd.* 383, 1-2 (2004), 184–188. <https://doi.org/10.1016/j.jallcom.2004.04.053>
- [23] Christoph Klein, János Sallai, Trevor J Jones, Christopher R Iacobella, Clare McCabe, and Peter T Cummings. 2016. A Hierarchical, Component Based Approach to Screening Properties of Soft Matter. *Found. Mol. Model. Simul.* (2016). [https://doi.org/10.1007/978-981-10-1128-3\\_5](https://doi.org/10.1007/978-981-10-1128-3_5)
- [24] Thomas Kluyver, Benjamin Ragan-kelley, Fernando Pérez, Brian Granger, Matthias Bussonnier, Jonathan Frederic, Kyle Kelley, Jessica Hamrick, Jason Grout, Sylvain Corlay, Paul Ivanov, Damián Avila, Safia Abdalla, and Carol Willing. 2016. Jupyter Notebooks - A Publishing Format for Reproducible Computational Workflows. *Position. Power Acad. Publ. Play. Agents Agendas* (2016), 87–90. <https://doi.org/10.3233/978-1-61499-649-1-87>
- [25] Gongping Liu, Fenjuan Xiangli, Wang Wei, Sainan Liu, and Wanqin Jin. 2011. Improved performance of PDMS/ceramic composite pervaporation membranes by ZSM-5 homogeneously dispersed in PDMS via a surface graft/coating approach. *Chem. Eng. J.* 174, 2-3 (2011), 495–503. <https://doi.org/10.1016/j.cej.2011.06.004>
- [26] Evan Miller, Matthew Jones, and Eric Jankowski. 2018. Tying Together Multiscale Calculations for Charge Transport in P3HT: Structural Descriptors, Morphology, and Tie-Chains. *Polymers (Basel)*. 10, 12 (dec 2018), 1358. <https://doi.org/10.3390/polym10121358>
- [27] Evan D Miller, Matthew Lewis Jones, Michael M Henry, Paul Chery, Kyle Miller, and Eric Jankowski. 2018. Optimization and Validation of Efficient Models for Predicting Polythiophene Self-Assembly. *Polymers (Basel)*. 10, 12 (nov 2018), 1305. <https://doi.org/10.3390/polym10121305>
- [28] Evan D Miller, Matthew Lewis Jones, and Eric Jankowski. 2017. Enhanced Computational Sampling of Perylene and Perylothiophene Packing with Rigid-Body Models. *ACS Omega* 2, 1 (jan 2017), 353–362. <https://doi.org/10.1021/acsomega.6b00371>
- [29] P. Müllner, V. A. Chernenko, M. Wollgarten, and G. Kostorz. 2002. Large cyclic deformation of a Ni-Mn-Ga shape memory alloy induced by magnetic fields. *J. Appl. Phys.* 92, 11 (2002), 6708–6713. <https://doi.org/10.1063/1.1513875>
- [30] S. J. Murray, M. Marioni, S. M. Allen, R. C. O'Handley, and T. A. Lograsso. 2000. 6% magnetic-field-induced strain by twin-boundary motion in ferromagnetic Ni-Mn-Ga. *Appl. Phys. Lett.* 77, 6 (2000), 886–888. <https://doi.org/10.1063/1.1306635>
- [31] NCSA. 2018. About Blue Waters. <http://www.ncsa.illinois.edu/>
- [32] C. Seguí, V. A. Chernenko, J. Pons, E. Cesari, V. Khovailo, and T. Takagi. 2005. Low temperature-induced intermartensitic phase transformations in Ni-Mn-Ga single crystal. *Acta Mater.* 53, 1 (2005), 111–120. <https://doi.org/10.1016/j.actamat.2004.09.008>
- [33] Aaron R. Smith, Andrey Saren, Jari Järvinen, and Kari Ullakko. 2015. Characterization of a High-Resolution Solid-State Micropump that can be Integrated into Microfluidic Systems. *Microfluid. Nanofluidics* 18, 5-6 (may 2015), 1255–1263. <https://doi.org/10.1007/s10404-014-1524-6>
- [34] A Sozinov, A.A. Likhachev, and K Ullakko. 2002. Crystal Structures and Magnetic Anisotropy Properties of Ni-Mn-Ga Martensitic Phases with Giant Magnetic-Field-Induced Strain. *IEEE Trans. Magn.* 38, 5 (sep 2002), 2814–2816. <https://doi.org/10.1109/TMAG.2002.803567>
- [35] L. Straka, A. Soroka, H. Seiner, H. Hänninen, and A. Sozinov. 2012. Temperature dependence of twinning stress of Type I and Type II twins in 10M modulated Ni-Mn-Ga martensite. *Scr. Mater.* 67, 1 (2012), 25–28. <https://doi.org/10.1016/j.scriptamat.2012.03.012>
- [36] Yoshinori Tamai, Hideki Tanaka, and Koichiro Nakanishi. 1994. Molecular Simulation of Permeation of Small Penetrants through Membranes. 1. Diffusion Coefficients. *Macromolecules* 27, 16 (aug 1994), 4498–4508. <https://doi.org/10.1021/ma00094a011>
- [37] Mesfin Tsige, Thomas Sodemann, Susan B. Rempe, Gary S. Crest, Joel D. Kress, Mark O. Robbins, Scott W. Sides, Mark J. Stevens, and Edmund Webb. 2003. Interactions and structure of poly(dimethylsiloxane) at silicon dioxide surfaces: Electronic structure and molecular dynamics studies. *J. Chem. Phys.* 118, 11 (2003), 5132–5142. <https://doi.org/10.1063/1.1545091>
- [38] K. Ullakko, J. K. Huang, C. Kantner, R. C. O'Handley, and V. V. Kokorin. 1996. Large magnetic-field-induced strains in Ni<sub>2</sub>MnGa single crystals. *Appl. Phys. Lett.* 69, 13 (1996), 1966–1968. <https://doi.org/10.1063/1.117637>